The University of Sydney

School of Civil Engineering
Sydney NSW 2006
AUSTRALIA

http://www.civil.usyd.edu.au/

Environmental Fluids/Wind Group

Dynamic Analysis of an Infinite Cylindrical Hole in a Saturated Porous Medium

Research Report No R865

Frank Lu, BE ME PhD
Dong-Sheng Jeng, BE ME PhD

April 2006

ISSN 1833-2781

The University of Sydney

School of Civil Engineering
Environmental Fluids/Wind Group
http://www.civil.usyd.edu.au/

Dynamic Analysis of An infinite Cylindrical Hole in a Saturated Porous Medium

Research Report No R865

Frank Lu, BE ME PhD
Dong-Sheng Jeng, BE ME PhD

April 2006

Abstract:

In this study, the dynamic response of an infinite cylindrical hole embedded in a porous medium and subjected to an axisymmetric ring load is investigated. Two scalar potentials and two vector potentials are introduced to decouple the governing equations of Biot's theory. By taking a Fourier transform with respect to time and the axial coordinate, we derive general solutions for the potentials, displacements, stresses and pore pressures in the frequency-wave-number domain. Using the general solutions and a set of boundary conditions applied at the hole surface, the frequency-wave-number domain solutions for the proposed problem are determined. Numerical inversion of the Fourier transform with respect to the axial wave number yields the frequency domain solutions, while a double inverse Fourier transform with respect to frequency as well as the axial wave number generates the time-space domain solution. The numerical results of this paper indicate that the dynamic response of a porous medium surrounding an infinite hole is dependant upon many factors including the parameters of the porous media, the location of receivers, the boundary conditions along the surface of the hole as well as the load characteristics

Keywords:

porous media; infinite cylindrical hole; Biot's theory; Fourier transform

Copyright Notice

Department of Civil Engineering, Research Report R865
Dynamic Analysis of An infinite Cylindrical Hole in a Saturated Porous Medium

f.lu@civil.usyd.edu.au d.jeng@civil.usyd.edu.au

ISSN 1833-2781

Published by:
School of Civil Engineering
The University of Sydney
Sydney NSW 2006
AUSTRALIA

December 2005

This report and other Research Reports published by The School of Civil Engineering are available on the Internet:

http://www.civil.usyd.edu.au

Contents

1 Introduction#

The behavior of a cylindrical hole subjected to a dynamic load is of fundamental importance in transportation engineering, mining engineering and geophysical exploration. For example, the analysis of the dynamic impact of a gas explosion inside a mine on the surrounding rock is important in evaluating the damage caused by gas explosions. The dynamic analysis of a cylindrical hole subjected to a ring load is a vital task for borehole acoustics which mainly aims at parameter inversion.

To date, there have been numerous investigations regarding the analysis of a cylindrical hole subjected to dynamic or static loads. For the case of static loading, Tranter (1946) and Bowie (1947) investigated analytically the static response of a cylindrical hole subjected to radial pressure over a segment of the hole surface. Parnes (1983a) presented a static analysis of a cylindrical hole subjected to both pressure and torsional load. For dynamic loading, Selberg (1952) considered the dynamic response of a cylindrical hole subjected to a suddenly applied pressure along the entire surface of the hole. Jordan (1962) investigated the dynamic problem of a circular borehole subjected to an explosive pressure over a segment of the hole surface. Later, using dynamic elasticity theory and the Fourier transformation method, the response of an infinite elastic medium to a traveling load in a cylindrical borehole was presented by Parnes (1969). Parnes (1983b, 1986) further studied the dynamic response of a circular borehole loaded by a harmonic normal ring load and a harmonic torsional ring force. It is worth noting that all these investigations have been limited to the case of a single phase elastic medium.

Recently, a few researchers have attempted the quasi-static analysis of a circular hole embedded in a poroelastic medium. For example, based on Biot's consolidation theory as well as the Laplace and the Fourier transform method, a circular borehole embedded in a poroelastic medium and subjected to a static ring load was addressed by Rajapakse (1993). Using a decomposition scheme, the poroelastic solution for an inclined borehole was presented in Cui *et al.* (1997). However, the problem of a cylindrical hole in a poroelastic medium subjected to a dynamic ring load has not been considered to date.

In this study, based on Biot's dynamic theory (Biot, 1956a, 1956b, 1962), the response of the porous medium surrounding a cylindrical hole subjected to a dynamic ring load is investigated. In order to decouple the displacements of the solid frame and the pore fluid,

two scalar potentials and two vector potentials are introduced. Then, a Fourier transform is carried out to obtain the general solutions of the potentials. Using the general solutions and the boundary conditions at the hole surface, the response of the porous medium in the vicinity of an infinite hole can be determined. Based on the proposed model, a parametric study will be carried out with some detailed discussions.

2 Governing equations and general solutions

In general, there are four theories for porous media: Biot's theory (Biot, 1941, 1956a, 1956b, 1962); the mixture theory (Truesdell and Noll, 1965; Morland, 1972; Bowen, 1980, 1982; Passman *et al*., 1984) or the theory of porous media (TPM) (de Boer, 2000; Ehler and Bluhm, 2002); the viscoelastic model (O'Connell and Budiansky, 1977); and the micromechanics approach (Christensen, 1979; Hudson et al., 1996; Jakobsen et al., 2003; Mura, 1982; Nemat-Nasser, 1999). Among these, Biot's theory is a phenomenological theory, which is an intuitive extension of existing theories. This approach is appealing as it is built on an existing knowledge base. For engineering applications, the parameters involved in the model are firmly related to engineering experience. Therefore, Biot's theory has been commonly-used to model porous media problems, although some drawbacks of the theory have been reported. For example, in the framework of Biot's theory, the porosity is treated as a material constant rather than a variable. Moreover, the attenuation of the porous medium is not accounted for appropriately by Biot's theory. In addition, Biot's theory essentially belongs to a macroscopic theory, so it mainly holds for homogeneous porous media without microstructure. From a theoretical point of view, the mixture theory or the theory of porous media (TPM) are more appropriate models for addressing porous media: they are more rigorous than Biot's theory since the theories are based on the first principles of mechanics. However, the mixture theory and the theory of porous media are somehow too complicated for engineering applications. Thus, in this study, we apply Biot's theory to the present problem as a first approximation for engineering application.

2.1 Biot's theory and definition of the Fourier transform

The constitutive equations for a homogeneous porous medium can be expressed as (Biot, 1956a, 1956b, 1962)

$$\sigma_{ij} = 2\mu\varepsilon_{ij} + \lambda\delta_{ij}e - \alpha\delta_{ij}p \tag{1}$$

$$p = -\alpha M e + M\vartheta \tag{2}$$

$$e = u_{i,i}\,,\ \vartheta = -w_{i,i} \tag{3}$$

where u_i and w_i denote the average solid displacement and the infiltration displacement of the pore fluid respectively; ε_{ij} and e are the strain tensor and the dilatation of the solid skeleton; ϑ is the volume of fluid injected per unit volume of bulk material; σ_{ij} is the stress of the bulk material; p is the excess pore fluid pressure and δ_{ij} is the Kronecker delta. Moreover, λ and μ are Lame constants of the solid skeleton, respectively; α and M are two Biot parameters (Biot, 1941) accounting for the compressibility of the saturated porous medium. The expression for the fluid discharge in i-th ($i = x, y, z$) direction has the following form

$$q_i = \frac{\partial w_i}{\partial t} \tag{4}$$

The equation of motion for the bulk material and the pore fluid are expressed in terms of the displacements u_i and w_i

$$\mu u_{i,jj} + (\lambda + \alpha^2 M + \mu) u_{j,ji} + \alpha M w_{j,ji} = \rho_b \ddot{u}_i + \rho_f \ddot{w}_i\,, \tag{5a}$$

$$\alpha\ M u_{j,ji} + M w_{j,ji} = \rho_f u_i + m\ddot{w}_i + \frac{\eta}{k} K(t) * \dot{w}_i\,, \tag{5b}$$

where ρ_b, ρ_f denote the bulk density of the porous medium and the density of the pore fluid, $\rho_b = (1-\phi)\rho_s + \phi\rho_f$, ρ_s is the density of the solid skeleton and ϕ is the porosity of the porous medium; $m = a_\infty \rho_f / \phi$ and a_∞ is tortuosity; η, k account for the viscosity of the pore fluid and the permeability of the porous medium respectively, and $K(t)$ is a time dependent viscosity correction factor which describes the transition behavior from the viscosity dominated flow in low frequency range towards the inertia dominated flow in the high frequency range (Biot, 1956b; Johnson *et al*., 1987; Pride *et al*., 1993)); a superimposed dot on a variable denotes the derivative with respect to time and a star ($*$) between two variables denotes time convolution.

Here, we scale the problem with a reference length, shear modulus and density (a_R, μ_R, ρ_R). All geometrical and physical quantities are non-dimensionalised as follows

$$x_i^* = \frac{x_i}{a_R}, u_i^* = \frac{u_i}{a_R}, w_i^* = \frac{w_i}{a_R}, q_i^* = q_i\sqrt{\frac{\rho_R}{\mu_R}}, \eta^* = \frac{\eta}{a_R\sqrt{\mu_R \rho_R}},$$

$$k^* = \frac{k}{a_R^2}, \lambda^* = \frac{\lambda}{\mu_R}, \mu^* = \frac{\mu}{\mu_R}, M^* = \frac{M}{\mu_R}, F^* = \frac{F}{\mu_R a_R^2},$$

$$\rho_b^* = \frac{\rho_b}{\rho_R}, \rho_f^* = \frac{\rho_f}{\rho_R}, t^* = \frac{t}{a_R}\sqrt{\frac{\mu_R}{\rho_R}}, \ \omega^* = \omega a_R \sqrt{\frac{\rho_R}{\mu_R}} \tag{6}$$

where the quantities with asterisk are the non-dimensional quantities and F denotes force. To simplify the mathematical expressions, the non-dimensional geometrical and physical quantities in equation (6) will be used in the following sections. Furthermore, for simplicity, the superscript asterisks will be omitted in all quantities which follow.

To derive a general solution for Biot's equations in the cylindrical coordinate system, two kinds of Fourier transform are involved: the Fourier transform with respect to time and the Fourier transform with respect to the axial coordinate. In this paper, the Fourier transforms for both cases are defined as follows (Sneddon, 1951)

$$\hat{f}(\zeta) = \int_{-\infty}^{+\infty} f(x) e^{-i\zeta x} dx, \ f(x) = \frac{1}{2\pi} \int_{-\infty}^{+\infty} \hat{f}(\zeta) e^{i\zeta x} d\zeta \tag{7}$$

where x denotes time or the axial coordinate, while ζ represents frequency or the axial wave number, $i = \sqrt{-1}$.

2.2 The potentials for Biot's theory

To solve the above governing equations, the Helmholtz decomposition for the solid displacement and the infiltration displacement of the pore fluid is introduced. In a Cartesian coordinate system, therefore, the displacement of the solid skeleton and the infiltration displacement of the pore fluid have the following form

$$u_i = \varphi_{,i}^{(s)} + e_{ijk} \psi_{k,j}^{(s)} \tag{8a}$$

$$w_i = \varphi_{,i}^{(f)} + e_{ijk} \psi_{k,j}^{(f)} \tag{8b}$$

where $\varphi^{(s)}$ and $\psi_k^{(s)}$ (k=1, 2, 3) are the scalar and vector potentials for the solid displacement, while $\varphi^{(f)}$ and $\psi_k^{(f)}$ (k=1, 2, 3) are for the infiltration displacement of the pore fluid and e_{ijk} is the Levi-Civita symbol.

Substituting equation (8) into equation (5), together with the application of the Fourier transform on time, yields

$$(\lambda_c + 2\mu)\hat{\varphi}^{(s)}_{,jj} + \rho\omega^2\hat{\varphi}^{(s)} = -\alpha M\hat{\varphi}^{(f)}_{,jj} - \rho_f\omega^2\hat{\varphi}^{(f)} \tag{9a}$$

$$\alpha^2 M\hat{\varphi}^{(s)}_{,jj} + \alpha\rho_f\omega^2\hat{\varphi}^{(s)} = -\alpha M\hat{\varphi}^{(f)}_{,jj} - \alpha\beta_1\hat{\varphi}^{(f)} \tag{9b}$$

$$\hat{\psi}^{(s)}_{k,jj} + k_t^2\hat{\psi}^{(s)}_k = 0 \tag{9c}$$

$$\hat{\psi}^{(f)}_k = \beta_2\hat{\psi}^{(s)}_k \tag{9d}$$

where the caret denotes the Fourier transformation with respect to time, $\lambda_c = \lambda + \alpha^2 M$, $\beta_1 = m\omega^2 - i(\eta/k)\omega\hat{K}(\omega)$, $\beta_2 = -\rho_f\omega^2/\beta_1$ and k_t is the frequency-dependent complex wave number for the shear wave of the porous medium

$$k_t = \omega\sqrt{\frac{\rho_b + \beta_2\rho_f}{\mu}} \tag{10}$$

Note that to guarantee the attenuation of the elastic wave in the porous medium, the imaginary part of k_t should be non-positive for the Fourier transform defined in equation (7). Combining (9a) and (9b) gives the following expressions

$$\hat{\varphi}^{(f)} = \frac{\lambda + 2\mu}{\beta_3}\hat{\varphi}^{(s)}_{,jj} + \frac{\rho\omega^2 - \alpha\rho_f\omega^2}{\beta_3}\hat{\varphi}^{(s)} \tag{11a}$$

$$\hat{\varphi}^{(s)}_{,jjkk} + \varepsilon_1\hat{\varphi}^{(s)}_{,jj} + \varepsilon_2\hat{\varphi}^{(s)} = 0 \tag{11b}$$

in which $\varepsilon_1 = (\delta_2 + \delta_3 + \lambda_c + 2\mu)/\delta_1$, $\varepsilon_2 = (\delta_4 + \rho_b\omega^2)/\delta_1$, $\delta_1 = \alpha M(\lambda + 2\mu)/\beta_3$, $\delta_2 = \alpha M(\rho_b\omega^2 - \alpha\rho_f\omega^2)/\beta_3$, $\delta_3 = \rho_f\omega^2(\lambda + 2\mu)/\beta_3$, $\delta_4 = \rho_f\omega^2(\rho_b\omega^2 - \alpha\rho_f\omega^2)/\beta_3$, $\beta_3 = \alpha\beta_1 - \rho_f\omega^2$.

Equations (9) and (11) indicate that the potentials of the solid and the pore fluid are not independent of each other. That is, the potentials of the pore fluid can be derived from those of the solid skeleton. Moreover, the vector potential for the solid frame is determined by the Helmholtz equation (9c), which can be easily solved in a cylindrical coordinate system by Fourier transformation. In order to develop the general solution for the potential $\hat{\varphi}^{(s)}$, equation (11b) is rewritten in the following form

$$(\nabla^2 + k_f^2)(\nabla^2\hat{\varphi}^{(s)} + k_s^2\hat{\varphi}^{(s)}) = 0 \tag{12}$$

where ∇^2 is the Laplacian operator, $k_f^2 + k_s^2 = \varepsilon_1$, $k_f^2 k_s^2 = \varepsilon_2$, k_f, k_s are the frequency-dependent complex wave numbers for the fast and the slow P wave, respectively. By introducing potential $\hat{\chi}$, equation (12) is reduced to

$$\nabla^2\hat{\varphi}^{(s)} + k_s^2\hat{\varphi}^{(s)} = \hat{\chi} \tag{13a}$$

$$\nabla^2\hat{\chi} + k_f^2\hat{\chi} = 0 \tag{13b}$$

It follows from equation (13), that the general solution of the potential $\hat{\chi}$ is given by the Helmholtz equation (13b), while the general solution of $\hat{\varphi}^{(s)}$ is given by the inhomogeneous Helmholtz equation (13a).

2.3 General solutions in an axisymmetric cylindrical coordinate system

Since the dynamic ring load is axisymmetric, it is convenient to consider our problem in a cylindrical coordinate system (ρ,θ,z). If the axisymmetric condition is taken into account in the coordinate system (ρ,θ,z), the vector potential $\hat{\psi}_k^{(s)}$ and $\hat{\psi}_k^{(f)}$ can be represented by two scalar potentials, i.e., $\hat{\eta}^{(s)}$ and $\hat{\eta}^{(f)}$. As a result, the displacement for the solid skeleton and the infiltration displacement for the pore fluid are expressed as follows

$$\hat{u}_\rho = \frac{\partial\hat{\varphi}^{(s)}}{\partial\rho} + \frac{\partial^2\hat{\eta}^{(s)}}{\partial\rho\partial z},\ \hat{u}_z = \frac{\partial\hat{\varphi}^{(s)}}{\partial z} - \frac{1}{\rho}\frac{\partial}{\partial\rho}(\rho\frac{\partial\hat{\eta}^{(s)}}{\partial\rho}),$$

$$\hat{w}_\rho = \frac{\partial\hat{\varphi}^{(f)}}{\partial\rho} + \frac{\partial^2\hat{\eta}^{(f)}}{\partial\rho\partial z},\ \hat{w}_z = \frac{\partial\hat{\varphi}^{(f)}}{\partial z} - \frac{1}{\rho}\frac{\partial}{\partial\rho}(\rho\frac{\partial\hat{\eta}^{(f)}}{\partial\rho}) \tag{14}$$

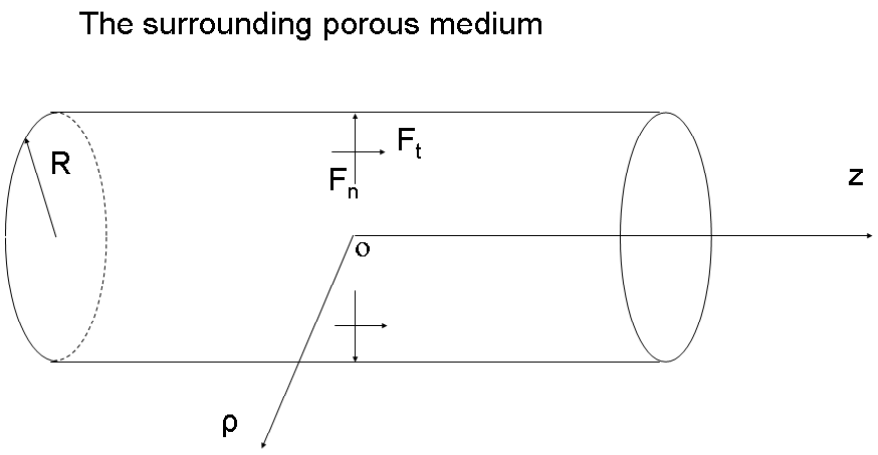

Figure 1: An infinite cylindrical hole in a porous medium subjected to a concentrated or uniformly distributed ring load.

where ρ, z are the radial and the axial coordinate, respectively (Figure 1), $\hat{\varphi}^{(s)},\hat{\varphi}^{(f)}$ are given by equations (11), (13), while the potentials $\hat{\eta}^{(s)},\hat{\eta}^{(f)}$ are determined by the following

equations

$$\nabla^2\hat{\eta}^{(s)} + k_t^2\hat{\eta}^{(s)} = 0 \tag{15a}$$

$$\hat{\eta}^{(f)} = \beta_2\hat{\eta}^{(s)} \tag{15b}$$

where the axisymmetric Laplacian operator is defined by $\nabla^2 = \partial^2/\partial\rho^2 + 1/\rho\partial/\partial\rho + \partial^2/\partial^2 z$.

Performing the Fourier transformation with respect to the axial coordinate (z) on equation (13b), one has

$$\frac{\partial^2\tilde{\chi}}{\partial\rho^2} + \frac{1}{\rho}\frac{\partial\tilde{\chi}}{\partial\rho} + (k_f^2 - \xi^2)\tilde{\chi} = 0 \tag{16}$$

where the tilde denotes the combination of the Fourier transformation with respect to time and the Fourier transformation with respect to the axial coordinate z; ξ is the axial wave number. Letting $\gamma_f^2 = k_f^2 - \xi^2$ and choosing the branch of γ_f to satisfy $\mathrm{Im}(\gamma_f) < 0$, then the general solution of equation (16) has the form

$$\tilde{\chi} = A(\omega,\xi)H_0^{(2)}(\gamma_f\rho) \tag{17}$$

where $A(\omega,\xi)$ is a arbitrary constant to be determined by the boundary conditions, $H_0^{(2)}(\bullet)$ denotes the second kind of the Hankel function of zero order. Similarly, performing the Fourier transformation to the coordinate z on equation (13a) leads to

$$\frac{\partial^2\tilde{\varphi}^{(s)}}{\partial\rho^2} + \frac{1}{\rho}\frac{\partial\tilde{\varphi}^{(s)}}{\partial\rho} + (k_s^2 - \xi^2)\tilde{\varphi}^{(s)} = \tilde{\chi} \tag{18}$$

Using solution (17), the general solution for equation (18) is obtained as follows

$$\tilde{\varphi}^{(s)} = \frac{A(\omega,\xi)}{k_s^2 - k_f^2}H_0^{(2)}(\gamma_f\rho) + B(\omega,\xi)H_0^{(2)}(\gamma_s\rho) \tag{19}$$

where $\gamma_s^2 = k_s^2 - \xi^2$ and $\mathrm{Im}(\gamma_s) < 0$, $B(\omega,\xi)$ is an arbitrary constant. Applying the Fourier transform to the coordinate z on equation (15a) yields the general solution for $\tilde{\eta}^{(s)}$

$$\tilde{\eta}^{(s)} = C(\omega,\xi)H_0^{(2)}(\gamma_t\rho) \tag{20}$$

where $\gamma_t^2 = k_t^2 - \xi^2$ with $\mathrm{Im}(\gamma_t) < 0$ and $C(\omega,\xi)$ is an arbitrary constant. In terms of (11a), (15b), (19), (20), the general solutions for the potentials of the pore fluids have the following form

$$\tilde{\varphi}^{(f)} = \frac{\alpha_2 - \alpha_1 k_f^2}{k_s^2 - k_f^2} A(\omega,\xi) H_0^{(2)}(\gamma_f \rho) + (\alpha_2 - \alpha_1 k_s^2) B(\omega,\xi) H_0^{(2)}(\gamma_s \rho) \tag{21a}$$

$$\tilde{\eta}^{(f)} = \beta_2 C(\omega,\xi) H_0^{(2)}(\gamma_t \rho) \tag{21b}$$

where $\alpha_1 = (\lambda + 2\mu)/\beta_3$, $\alpha_2 = (\rho\omega^2 - \alpha\rho_f\omega^2)/\beta_3$.

Once the potentials are determined, the displacement of the solid frame and the pore fluid, the stresses and the pore pressure can be further obtained as follows

$$\tilde{u}_\rho = \frac{\gamma_f A(\omega,\xi)}{k_f^2 - k_s^2} H_{1f}^{(2)} - \gamma_s B(\omega,\xi) H_{1s}^{(2)} - i\xi\gamma_t C(\omega,\xi) H_{1t}^{(2)} \tag{22a}$$

$$\tilde{u}_z = \frac{i\xi A(\omega,\xi)}{k_s^2 - k_f^2} H_{1f}^{(2)} + i\xi B(\omega,\xi) H_{0s}^{(2)} + \gamma_t^2 C(\omega,\xi) H_{0t}^{(2)} \tag{22b}$$

$$\tilde{w}_\rho = \frac{(\alpha_2 - \alpha_1 k_f^2)\gamma_f A(\omega,\xi)}{k_f^2 - k_s^2} H_{1f}^{(2)} - (\alpha_2 - \alpha_1 k_s^2)\gamma_s B(\omega,\xi) H_{1s}^{(2)} - i\xi\beta_2\gamma_t C(\omega,\xi) H_{1t}^{(2)} \tag{22c}$$

$$\begin{aligned}\tilde{w}_z = i\xi[&\frac{(\alpha_2 - \alpha_1 k_f^2) A(\omega,\xi)}{k_s^2 - k_f^2} H_{0f}^{(2)} + (\alpha_2 - \alpha_1 k_s^2) B(\omega,\xi) H_{0s}^{(2)}] \\ &+ \frac{\beta_2\gamma_t C(\omega,\xi)}{\rho} H_{1t}^{(2)} + \beta_2\gamma_t^2 C(\omega,\xi)[H_{0t}^{(2)} - \frac{1}{\rho\gamma_t} H_{1t}^{(2)}]\end{aligned} \tag{22d}$$

$$\begin{aligned}\tilde{\sigma}_{\rho\rho} = 2\mu[&\frac{\gamma_f^2 A(\omega,\xi)}{k_s^2 - k_f^2} H_{0f}^{(2)} - \frac{\gamma_f A(\omega,\xi)}{\rho(k_s^2 - k_f^2)} H_{1f}^{(2)} - \gamma_s^2 B(\omega,\xi) H_{0s}^{(2)} \\ &+ \frac{\gamma_s B(\omega,\xi)}{\rho} H_{1s}^{(2)} - i\xi\gamma_t^2 C(\omega,\xi) H_{0t}^{(2)} + \frac{i\xi\gamma_t C(\omega,\xi)}{\rho} H_{1t}^{(2)}] \\ &+ \lambda[\frac{k_f^2 A(\omega,\xi)}{k_f^2 - k_s^2} H_{0f}^{(2)} - k_s^2 B(\omega,\xi) H_{0s}^{(2)}]\end{aligned} \tag{22e}$$

$$\begin{aligned}\tilde{\sigma}_{z\rho} = \frac{\mu}{k_f^2 - k_s^2}[&2\mathrm{i}\xi\gamma_f A(\omega,\xi) H_{1f}^{(2)} + 2\mathrm{i}\xi\gamma_s k_s^2 B(\omega,\xi) H_{1s}^{(2)} \\ &-2i\xi\gamma_s k_f^2 B(\omega,\xi) H_{1s}^{(2)} - \xi^2\gamma_t k_s^2 C(\omega,\xi) H_{1t}^{(2)} + \xi^2\gamma_t k_f^2 C(\omega,\xi) H_{1t}^{(2)} \\ &+\gamma_t^3 k_s^2 C(\omega,\xi) H_{1t}^{(2)} - \gamma_t^3 k_f^2 C(\omega,\xi) H_{1t}^{(2)}]\end{aligned} \tag{22f}$$

$$\tilde{\sigma}_{\theta\theta} = \frac{2\mu}{\rho}[\frac{\gamma_f A(\omega,\xi)}{k_f^2 - k_s^2} H_{1f}^{(2)} - \gamma_s B(\omega,\xi) H_{1s}^{(2)} - \mathrm{i}\xi\gamma_t C(\omega,\xi) H_{1t}^{(2)}]$$

$$+\lambda[\frac{k_f^2 A(\omega,\xi)}{k_f^2-k_s^2}H_{0f}^{(2)}-k_s^2 B(\omega,\xi)H_{0s}^{(2)}] \tag{22g}$$

$$\tilde{p}=\frac{\alpha M k_s^2 A(\omega,\xi)}{k_s^2-k_f^2}H_{0f}^{(2)}+\alpha M k_s^2 B(\omega,\xi)H_{0s}^{(2)}+\frac{M k_f^2(\alpha_2-\alpha_1 k_f^2)A(\omega,\xi)}{k_s^2-k_f^2}H_{0f}^{(2)}$$

$$-M(\alpha_2-\alpha_1 k_s^2)k_s^2 B(\omega,\xi)H_{0s}^{(2)} \tag{22h}$$

where $H_{nf}^{(2)}\equiv H_{nf}^{(2)}(\rho\gamma_f)$, $H_{ns}^{(2)}\equiv H_{ns}^{(2)}(\rho\gamma_s)$ and $H_{nt}^{(2)}\equiv H_{nt}^{(2)}(\rho\gamma_t)$, $n=0,1$.

3 Boundary value problems and the corresponding solutions

A cylindrical hole with radius (R) embedded in an infinite isotropic porous medium is considered here. The surface of the cylindrical hole is subjected to a normal or a tangential axisymmetric ring load, which can either be concentrated along a circle or uniformly distributed over a segment of the hole surface. Using the general solutions derived in the above section and the boundary conditions along the hole surface, the boundary value problems can be formulated in the frequency-wave-number domain. Then, the solution of the boundary value problems yields the three arbitrary constants involved in the general solutions.

If a concentrated normal or a tangential ring load F_n, F_t with axial coordinate $z=0$ is applied at the hole surface, then, the boundary conditions have the following form

$$\sigma_{\rho\rho}(R,z,t)=-\frac{F_n(t)}{2\pi R}\delta(z) \tag{23a}$$

$$\sigma_{z\rho}(R,z,t)=-\frac{F_t(t)}{2\pi R}\delta(z) \tag{23b}$$

where $\delta(\bullet)$ is the Dirac-δ function.

If the load is distributed over a segment of length $2d$, then, the boundary conditions can be expressed as follows

$$\sigma_{\rho\rho}(R,z,t)=-p_n(t)[H(z+d)-H(z-d)] \tag{24a}$$

$$\sigma_{z\rho}(R,z,t)=-p_t(t)[H(z+d)-H(z-d)] \tag{24b}$$

where $H(\bullet)$ is the Heaviside function and $p_n(t), p_t(t)$ are the time-dependent intensities of the normal and tangential traction applied at the hole surface.

If the hole surface is completely permeable, the pore pressure along the hole surface should vanish

$$p(R,z,t)=0 \tag{25}$$

On the other hand, if the hole surface is fully impermeable, then, the following boundary condition holds

$$q_\rho(R,z,t)=\frac{\partial w_\rho(R,z,t)}{\partial t}=0 \tag{26}$$

Performing a double Fourier transformation with respect to *z* and *t* on equation (23), the corresponding boundary conditions in the frequency-wave-number domain are obtained as follows

$$\tilde{\sigma}_{\rho\rho}(R,\xi,\omega)=-\frac{\tilde{F}_n(\omega)}{2\pi R} \tag{27a}$$

$$\tilde{\sigma}_{z\rho}(R,\xi,\omega)=-\frac{\tilde{F}_t(\omega)}{2\pi R} \tag{27b}$$

Similarly, double Fourier transformation of equation (24) leads to the following boundary conditions in the frequency-wave-number domain

$$\tilde{\sigma}_{\rho\rho}(R,\xi,\omega)=-2\tilde{p}_n(\omega)\frac{\sin(\xi \mathrm{d})}{\xi} \tag{28a}$$

$$\tilde{\sigma}_{z\rho}(R,\xi,\omega)=-2\,\tilde{p}_t(\omega)\frac{\sin(\xi \mathrm{d})}{\xi} \tag{28b}$$

In addition, in the frequency-wave-number domain, the permeable and the impermeable hydrodynamic boundary conditions have the form

$$\tilde{p}(R,\xi,\omega)=0 \tag{29a}$$

$$\tilde{q}_\rho(R,\xi,\omega)=i\omega\tilde{w}_\rho(R,\xi,\omega)=0 \tag{29b}$$

By using equations (27) or (28), (29) and equation (22), the arbitrary constants $A(\omega,\xi)$, $B(\omega,\xi)$, $C(\omega,\xi)$ in equation (22) can be calculated. For the concentrated normal ring load $\tilde{F}_n(\omega)$ ($\tilde{F}_t(\omega)=0$), the expressions for the three arbitrary constants, $A(\omega,\xi)$, $B(\omega,\xi)$, $C(\omega,\xi)$ are given in the Appendix. Substituting the obtained constants $A(\omega,\xi)$, $B(\omega,\xi)$, $C(\omega,\xi)$ into equation (22), the displacements, stresses and the pore pressure in the frequency-wave-number domain are obtained.

In order to show the implementation of the double inverse Fourier transform on the variables in equation (22), we shall use $\tilde{\Omega}$ to denote all the variables. Supposing the hole is subjected to a concentrated normal ring load, then, the expression of $\tilde{\Omega}$ can be written as follows

$$\tilde{\Omega}(\rho,\xi,\omega) = -\frac{\tilde{F}_n(\omega)}{2\pi R}\tilde{\Omega}^*(\rho,\xi,\omega) \tag{30}$$

The integral representation for $\Omega(\rho,z,t)$ in the time-space domain has the following form

$$\Omega(\rho,z,t) = \frac{1}{(2\pi)^2}\int_{-\infty}^{+\infty}\int_{-\infty}^{+\infty}(-\frac{1}{2\pi R})\tilde{F}_n(\omega)\tilde{\Omega}^*(\rho,\xi,\omega)e^{i(\omega t+\xi z)}d\xi d\omega \tag{31}$$

It follows from (31) that the time-space domain solution can be recovered by the double inverse Fourier transform with respect to ω,ξ on the frequency-wave-number domain solution. For loads with finite frequency band width, the integration with respect to ω can be evaluated by the FFT method (Oppenhein and Schafer, 1999), while the inverse Fourier transformation with respect to the axial wave number ξ can be accomplished by a direct numerical integration.

4 Results and Discussions

The frequency-wave-number domain solutions of the proposed problem are listed in equation (22), while the time-space domain solutions are represented by an infinite integral (31). The integral with respect to the axial wave number ξ is calculated using a subroutine in IMSL. Since the drag force between the solid skeleton and the pore fluid is dissipative, all the branch points and poles are complex. Thus, the infinite integral (31) with respect to the axial wave number ξ is free of any singularities in the path of integration.

For a high frequency signal, the low frequency Biot's theory (Biot, 1056a) is not suitable. In order to treat low and high frequency signals consistently, the JKD model (Johnson et al., 1987) is incorporated with Biot's theory (Biot, 1956b) in the current study. The JKD model can give an adequate approximation for many porous media (Johnson *et al*., 1987; Pride *et al*., 1993). The complex frequency dependent viscosity correction function in the JKD model has the form (Johnson *et al*., 1987)

$$\tilde{K}(\omega) = (1+i\frac{\omega}{\omega_c}\alpha_g)^{1/2}, \qquad \omega_c = \frac{\eta\phi}{\rho_f a_\infty k} \tag{33}$$

where ω_c is the transition frequency which separates the viscous-force-dominated flow from the inertial-force-dominated flow and α_g is the pore geometry term which is commonly equal to ½ for many porous media [28, 29].

In addition, in the following calculations, the reference length, shear modulus and density are chosen as follows

$$a_R = R\,,\ \mu_R = \mu\,,\ \rho_R = \rho_f \tag{34}$$

4.1 Comparisons with single-phase elastic model

Since the poro-elastic model for the present model is new and no experimental data is available, it is necessary to reduce the present model to single phase elastic model and compare with the previous model (Parnes, 1986). Allowing $\phi,\ \alpha, M, \eta$ to approach zero and k to approach infinity, then the present poroelastic model can be reduced to a single phase elastic model. In order to verify the present approach numerically, the results from the reduced single phase model are compared with results from the real single phase model (Parnes, 1986). The input data used in Parnes (1986) are used in the comparison. In the example, the tunnel surface is subjected to a normal ring load. Poisson's ratio of the elastic media surrounding the tunnel is equal to 0.25 and the non-dimensional angular frequency $\Omega = 2.0$. The results of the radial displacement and the loop stress for the real single phase model are taken from Figures 4 and 6 in the original paper (Parnes, 1986). Figure 2 illustrates the comparison of the results for the radial displacement and the loop stress along the radial direction for points $\rho = 1.5 - 5.0,\ z = 0$ between the two models. As show in the figure, the present model agrees well with Parnes's model (Parnes, 1986) for the case of single-phase elastic medium.

4.2 Dynamic response of the points with $0 \le z \le 22.5$ and ρ=1.5 in the frequency domain

In this section, the dynamic response of the points with $0.0 \le z \le 22.5$ and $\rho = 1.5$ to a normal concentrated ring load with magnitude F_n located at $z = 0$ is calculated. The material parameters are chosen as follows: $\mu = 1.0,\ \lambda = 0.3333,\ \rho_s = 2.5,\ \rho_f = 1.0\,,\ \ \phi = 0.3,$ $\alpha = 0.95\,, M = 0.6667\,,\ \eta = 5.774\times10^{-10},\ k = 1.0\times10^{-12},\ \phi = 0.3.$ The radius of the hole is $R = 1.0$ and its surface is assumed to be permeable. Three cases corresponding to

$\omega = 0.0, 4.0, 8.0$ are calculated. Figure 3 illustrates the variation of the amplitudes of $u_\rho / F_n, u_z / F_n, \sigma_{\theta\theta} / F_n, p / F_n$ versus the axial coordinate z for the three cases.

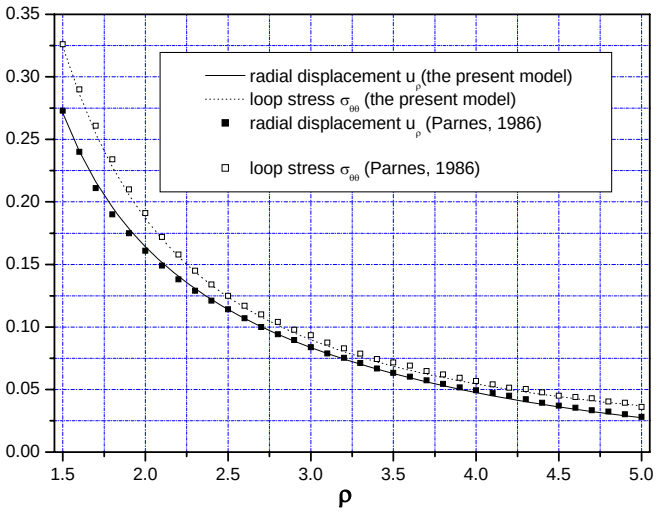

Figure 2: The comparison of the radial displacement and the loop stress due to a ring load applied at the surface of the cylindrical hole between our model and the single phase elastic model (Parnes, 1986).

Figure 3 shows that for the normal load, the amplitudes of $u_\rho / F_n, u_z / F_n, \sigma_{\theta\theta} / F_n, p / F_n$ decrease with increasing axial coordinate z for all three cases. It should be noted that the amplitudes of $u_\rho / F_n, u_z / F_n, \sigma_{\theta\theta} / F_n, p / F_n$ for the static case ($\omega = 0.0$) decrease faster than the other two cases. Also, the amplitudes of $u_\rho / F_n, u_z / F_n, \sigma_{\theta\theta} / F_n, p / F_n$ at receivers near the source ($z = 0.0$) vary more rapidly than the points further from the source, which can be explained by the fact that when receivers are placed near the source point, the body waves of the porous medium are dominant; however, for points further from the source, the pseudo-Rayleigh wave which is free of geometrical attenuation is dominant. Moreover, when frequency increases, the wave characteristics of $u_\rho / F_n, u_z / F_n, \sigma_{\theta\theta} / F_n, p / F_n$ becomes more pronounced. Figure 3 (a) and Figure 3 (b) indicate that the axial displacement u_z exhibits more wave characteristic than the radial displacement u_ρ does.

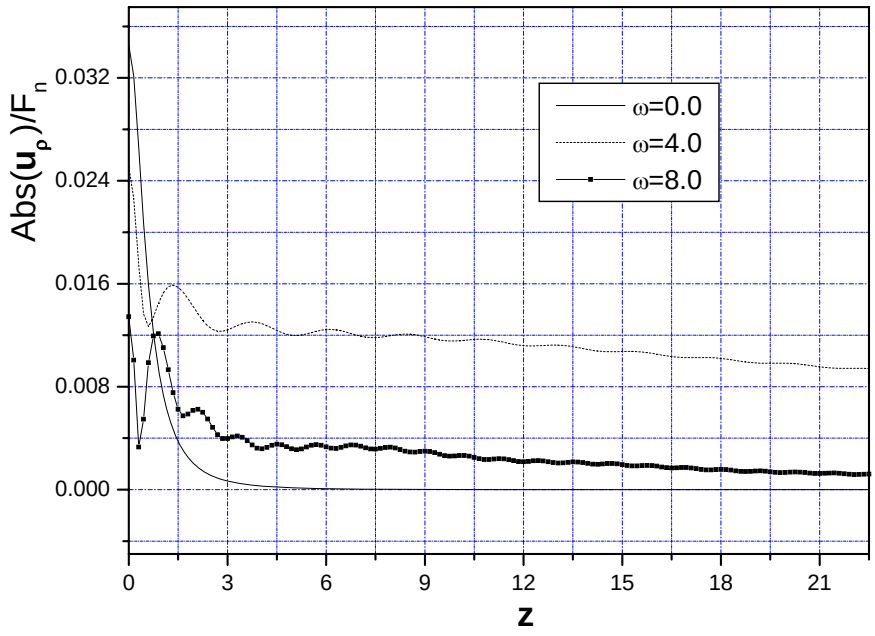

(a)

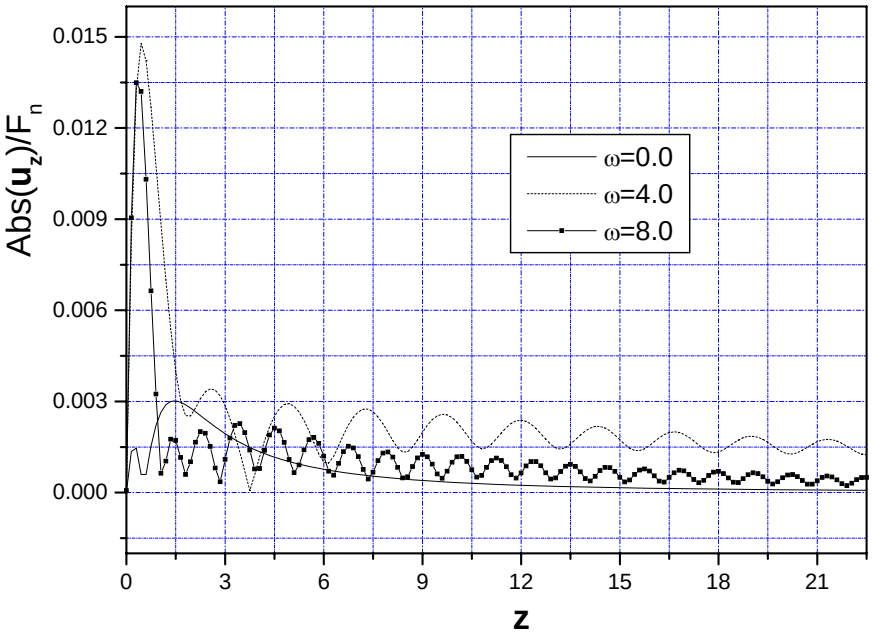

(b)

Figure 3(a)-(b): Frequency domain response of the points with $0.0 \le z \le 22.5$ and $\rho = 1.5$ near a permeable cylindrical hole surface subjected to a normal concentrated ring load F_n located at $z = 0.0$ with $\omega = 0$, 4, and 8.

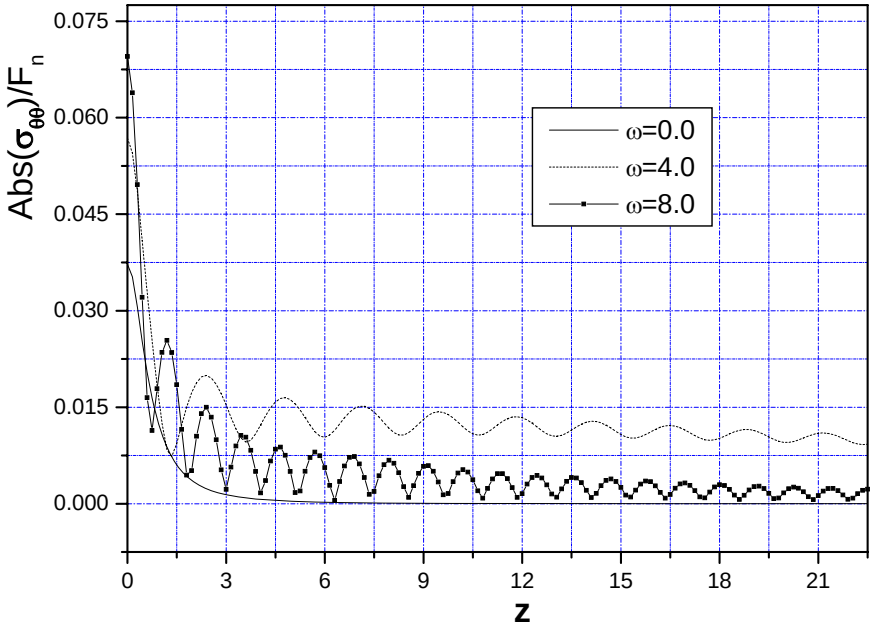

(c)

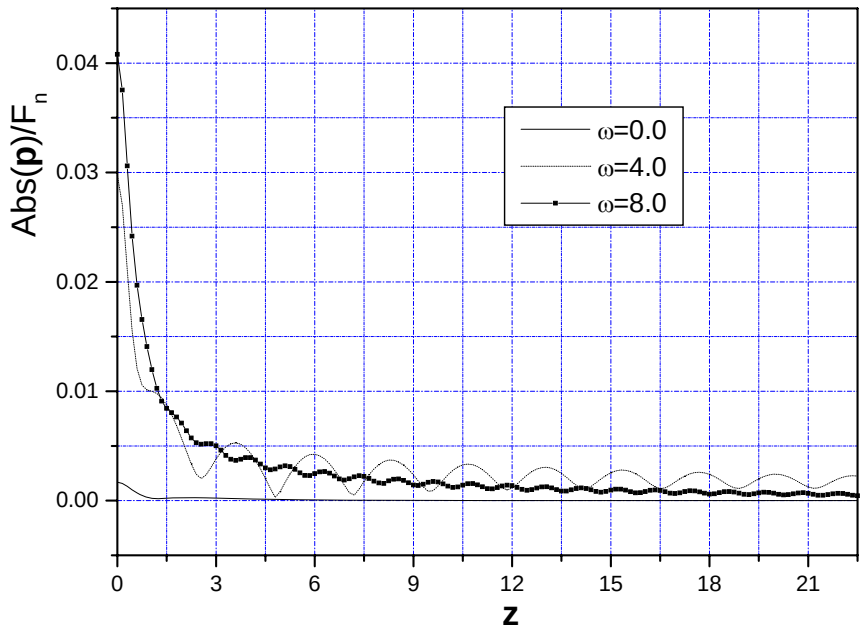

(d)

Figure 3(c)-(d): Frequency domain response of the points with $0.0 \le z \le 22.5$ and $\rho = 1.5$ near a permeable cylindrical hole surface subjected to a normal concentrated ring load F_n located at $z = 0.0$ with $\omega = 0$, 4, and 8.

4.3 The influence of frequency on the dynamic response of the points with $z = 5.0$ and $\rho = 1.5$

In this section, the influence of frequency on the dynamic response of the points with $z = 5.0$ and $\rho = 1.5$ is considered. The load is a normal concentrated ring force located at $z = 0$ with intensity F_n and the radius of the cylindrical hole is $R = 1.0$. The frequency ω of the normal ring load ranges between 0 and 18. The material parameters are chosen as follows: $\mu = 1.0$, $\lambda = 0.3333$, $\rho_s = 2.5$, $\rho_f = 1.0$, $\phi = 0.3$, $\alpha = 0.95$, $M = 0.6667$, $\eta = 5.774 \times 10^{-10}$, $\phi = 0.3$. Three cases corresponding to permeability $k = 1.0 \times 10^{-10}$, $k = 1.0 \times 10^{-11}$ and $k = 1.0 \times 10^{-12}$ for permeable and impermeable boundary are calculated.

Figures 4 and 5 plot the amplitudes of $u_\rho / F_n, u_z / F_n, \sigma_{\theta\theta} / F_n, p / F_n$ at the points for the permeable and impermeable boundary condition. As shown in Figures 4 (a) and 5 (a), for the radial displacement there is only one peak occurring in the calculation frequency range, which indicates resonance only takes place once for the radial displacement. Moreover, the radial displacement for the case $k = 1.0 \times 10^{-12}$ is the largest of the three cases. For the cases $k = 1.0 \times 10^{-10}$ and 1.0×10^{-11}, the maximum radial displacements of the permeable boundary case are slightly larger than those for the impermeable case. For the axial displacement u_z, low frequency resonance phenomenon is much more obvious than u_ρ. The amplitude of u_z appears to have several peaks at the lower frequency range. However, when frequency is larger than 14.0 (Figures 4 (b) and 5 (b)), the resonance phenomenon fades away. For the cases $k = 1.0 \times 10^{-11}$, 1.0×10^{-12}, $\sigma_{\theta\theta}, p$ also exhibits low frequency resonance phenomenon, while for the case $k = 1.0 \times 10^{-10}$, $\sigma_{\theta\theta}, p$ shows resonance phenomenon over the entire calculated frequency range. For the case $k = 1.0 \times 10^{-10}$, the maximum pore pressure p of the permeable boundary is larger than in the impermeable case. For the cases of $k = 1.0 \times 10^{-11}, 1.0 \times 10^{-12}$, the pore pressures p of the permeable and the impermeable boundary are very close to each other in lower frequency range. However, at higher frequencies, the pore pressures p of the impermeable boundary case is slightly larger than that of the permeable case.

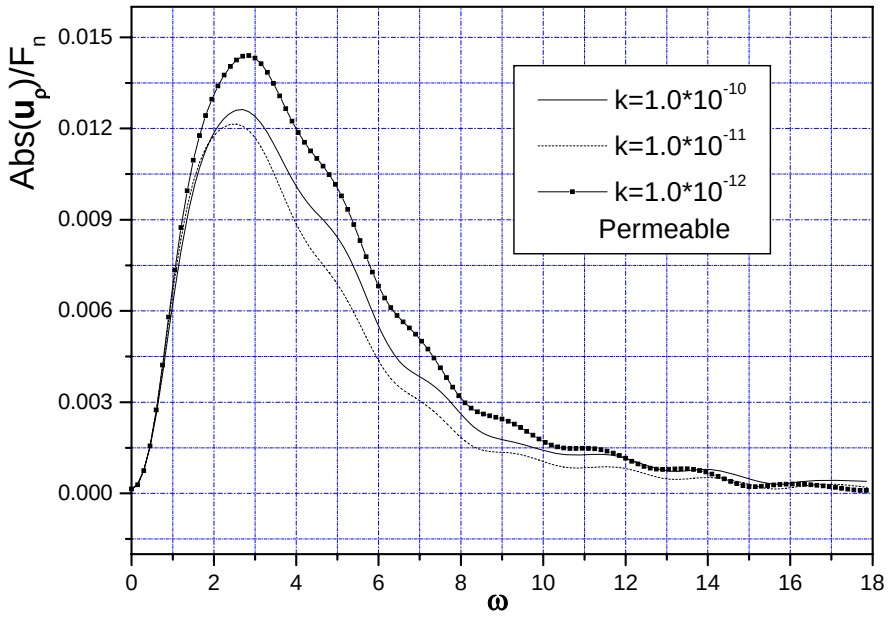

(a)

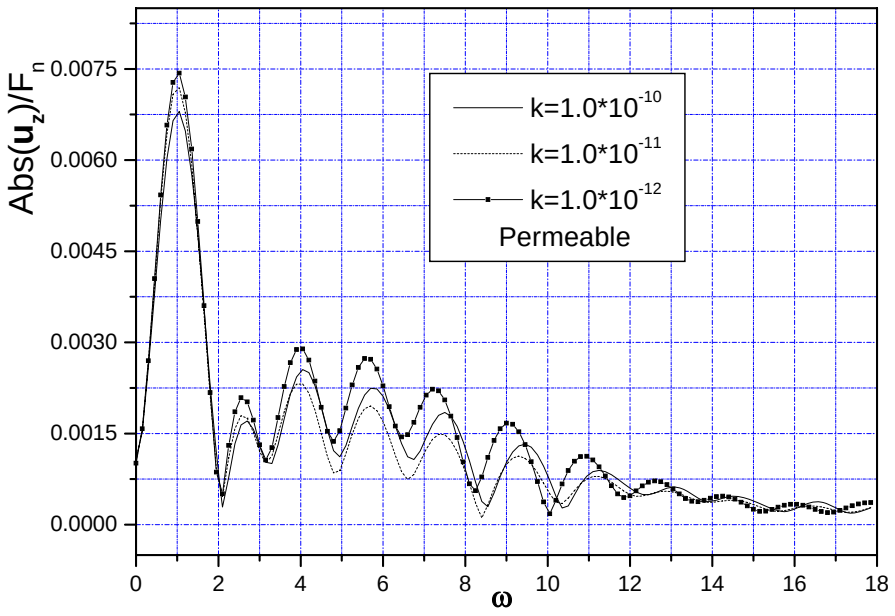

(b)

Figure 4(a)-(b): Frequency domain response at the points $z = 5.0$ and $\rho = 1.5$ with a permeable hole surface subjected to a normal ring load F_n located at $z = 0.0$ with $\omega = 0.0 \sim 18.0$.

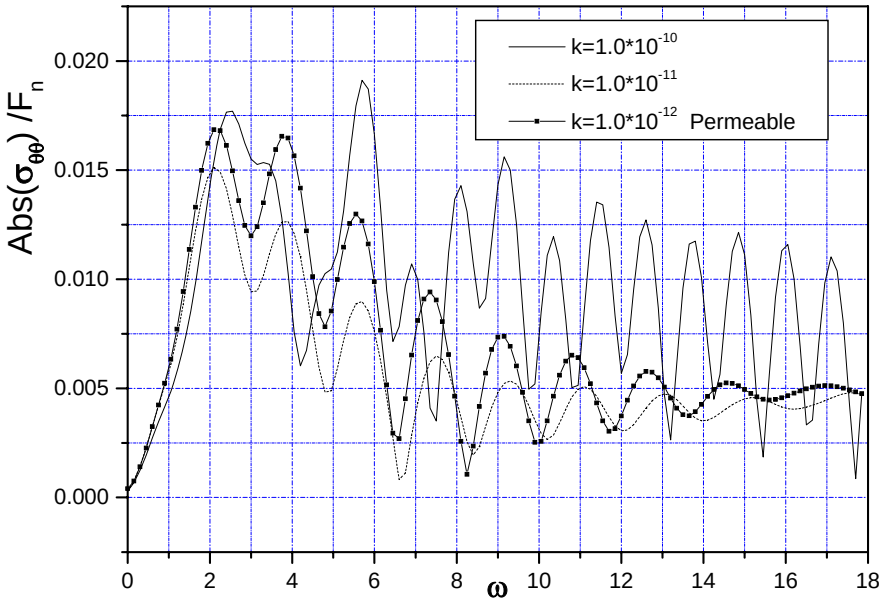

(c)

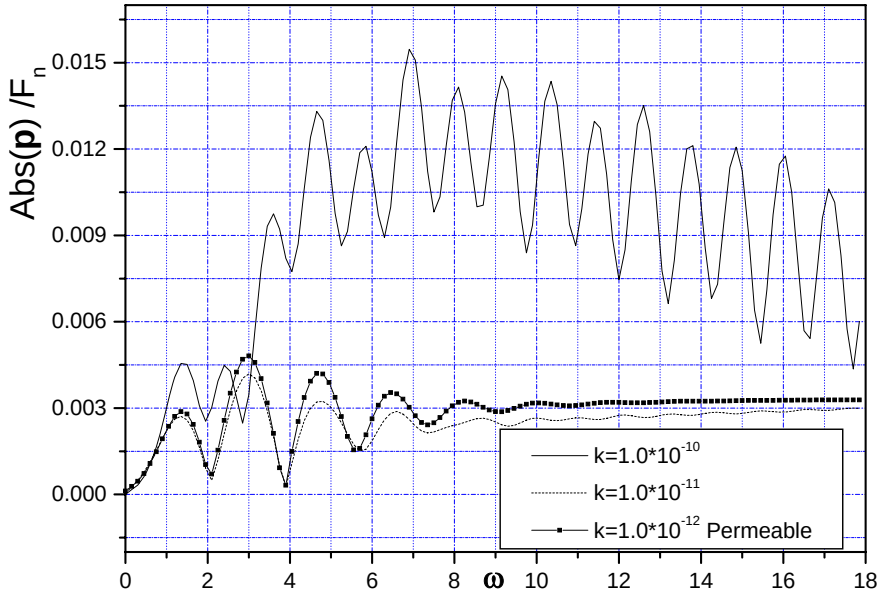

(d)

Figure 4(c)-(d): Frequency domain response at the points $z = 5.0$ and $\rho = 1.5$ with a permeable hole surface subjected to a normal ring load F_n located at $z = 0.0$ with $\omega = 0.0 \sim 18.0$.

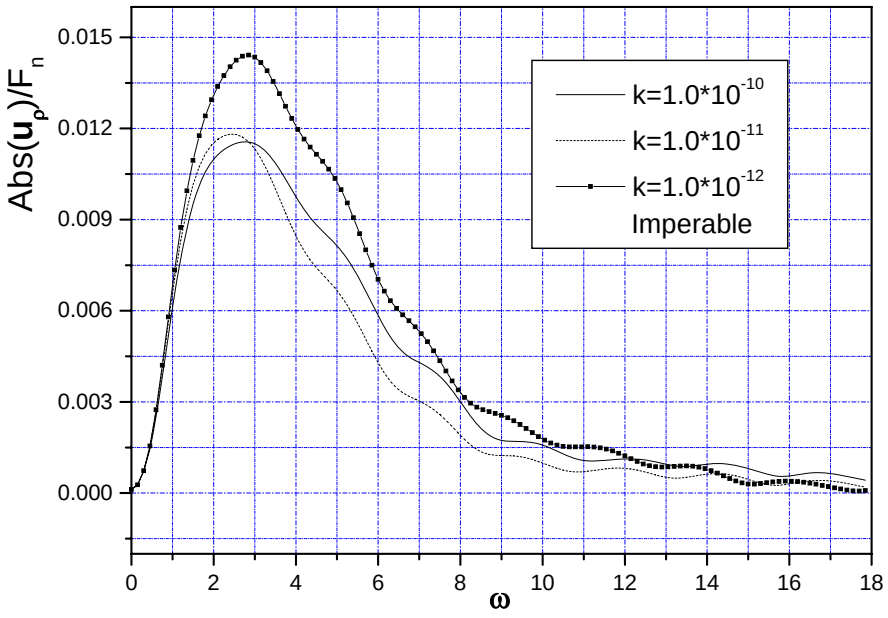

(a)

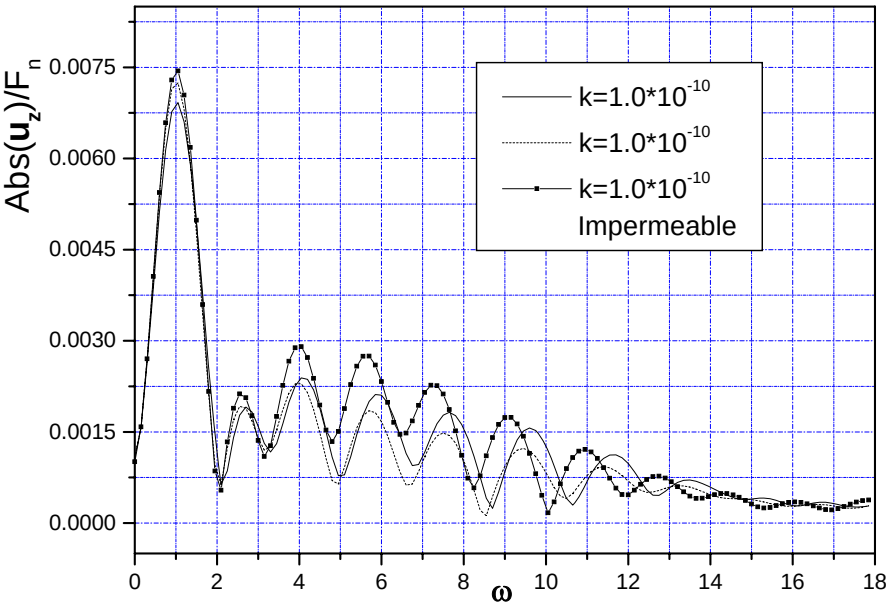

(b)

Figure 5(a)-(b): Frequency domain response at the points with $z = 5.0$ and $\rho = 1.5$ near a impermeable cylindrical hole surface subjected to a normal ring load F_n located at $z = 0.0$ with $\omega = 0.0 \sim 18.0$.

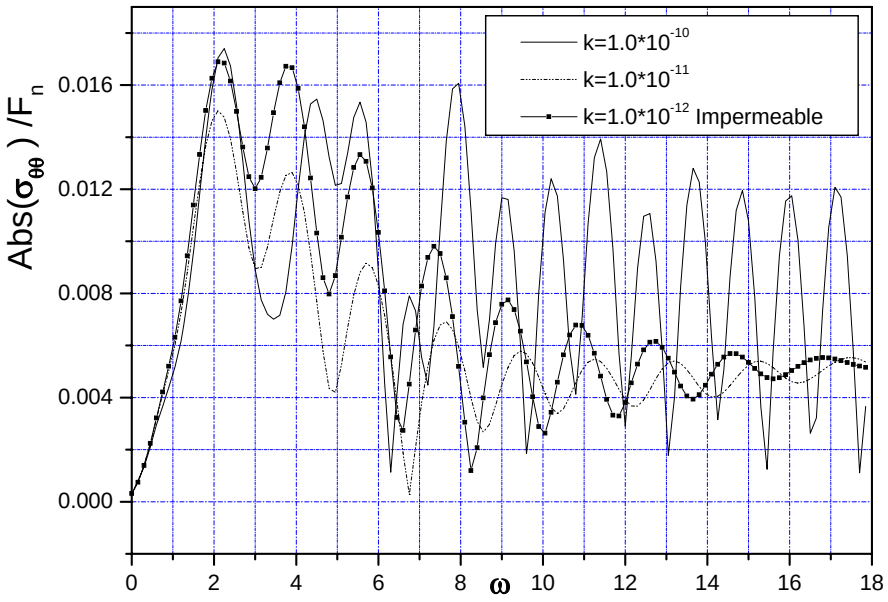

(c)

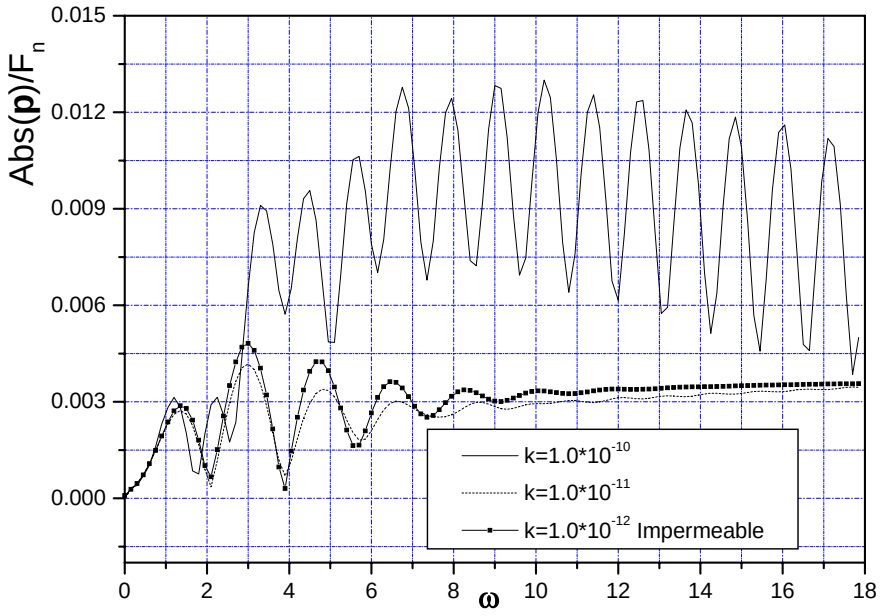

(d)

Figure 5(c)-(d): Frequency domain response at the points with $z = 5.0$ and $\rho = 1.5$ near a impermeable cylindrical hole surface subjected to a normal ring load F_n located at $z = 0.0$ with $\omega = 0.0 \sim 18.0$.

4.4 The influence of the radial position on the dynamic response of receivers in the time domain

In this section, the influence of the radial position of the receivers on the time domain response will be investigated. The time domain responses of three points with coordinates $z = 15.0$ and $\rho = 1.5, 4.0, 8.0$ respectively, are calculated. The radius of the cylindrical hole is $R = 1.0$ and the surface of the cylindrical hole is assumed to be permeable. The load is a concentrated normal ring load located at $z = 0$ and of the Ricker wavelet type (Ricker, 1977)

$$F_n(t) = F_n[\frac{\omega_0^2 (t-t_s)^2}{2} - 1]\, e^{-\frac{\omega_0^2 (t-t_s)^2}{4}} \tag{35}$$

where $\omega_0 = 1.1547\pi$, $t_s = 2.5981$. The material parameters are chosen as follows: $\mu = 1.0,\ \lambda = 0.3333,\ \rho_s = 2.5,\ \rho_f = 1.0$, $\phi = 0.3$, $\alpha = 0.95, M = 0.6667$, $\eta = 5.774 \times 10^{-10}$, $k = 1.0 \times 10^{-11}$, $\phi = 0.3$. In performing the inverse FFT with respect to ω, the number of the sample points in the frequency domain is taken as 280 and $\Delta\omega = 8.0973 \times 10^{-2}$. Figure 6 details the values of $u_\rho / F_n, u_z / F_n, \sigma_{\theta\theta} / F_n, p / F_n$ at the three points versus non-dimensional time.

Figures 6 (b)-(d) clearly show the P1 wave arrives at the point ($z = 15.0$, $\rho = 1.5$) first, then the point ($z = 15.0$, $\rho = 4.0$) and then the point ($z = 15.0$, $\rho = 8.0$). Similarly, Figure 6 (a) and Figure 6 (c) indicates that the pseudo-Rayleigh wave arrives at the points ($z = 15.0$, $\rho = 1.5$), ($z = 15.0$, $\rho = 4.0$) and ($z = 15.0$, $\rho = 8.0$) in sequence. It follows from Figure 6 (b) that the S wave of the porous medium arrives at the receivers between the P1 wave and the pseudo-Rayleigh wave and it partly overlaps with the P1 wave.

For the radial displacements at the three points, the contribution from the pseudo-Rayleigh wave is dominant, while the contributions from P1 and S waves is very small. For the axial displacement at the point ($z = 15.0, \rho = 1.5$), the influence of the pseudo-Rayleigh wave is larger than that of the P1 wave. In addition, at the point ($z = 15.0, \rho = 4.0$), the contribution of the S wave is also visible via the axial displacement u_z. Figures 6 (b) and (c) shows that with increasing radial distance, the loop stress $\sigma_{\theta\theta}$ due to the pseudo-Rayleigh wave decreases faster than the axial displacement u_z. Figure 6 (c) also shows that the S wave has a very small influence on the loop stress $\sigma_{\theta\theta}$. With increasing radial distance, the pore pressure due to the pseudo-Rayleigh wave decreases more quickly than the other variables: it only visible at the point ($z = 15.0$, $\rho = 1.5$). Moreover, the S wave of the porous medium has

no contribution to the pore pressure, which agrees with Biot's theory. Also, due to the larger attenuation of the P2 wave, the influence of the P2 wave is invisible for all the calculated variables.

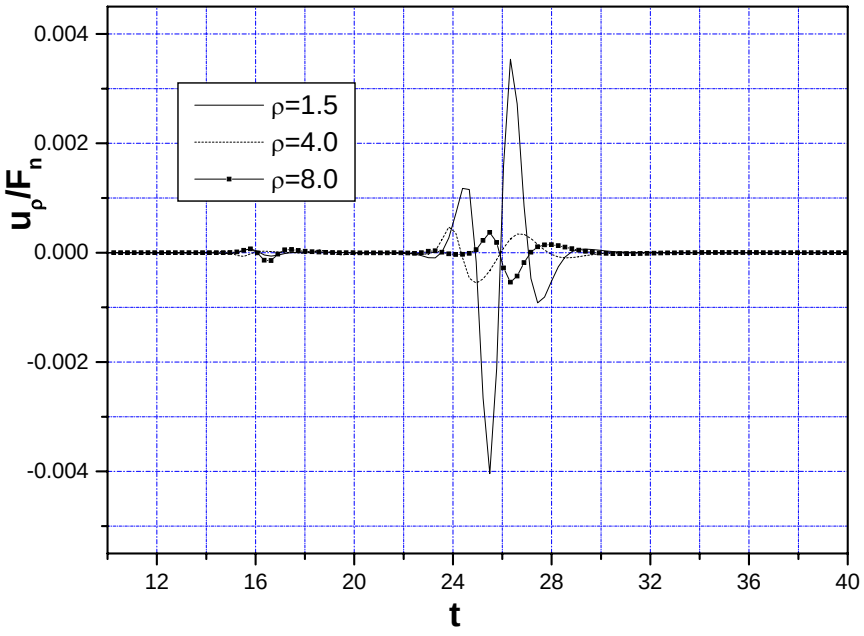

(a)

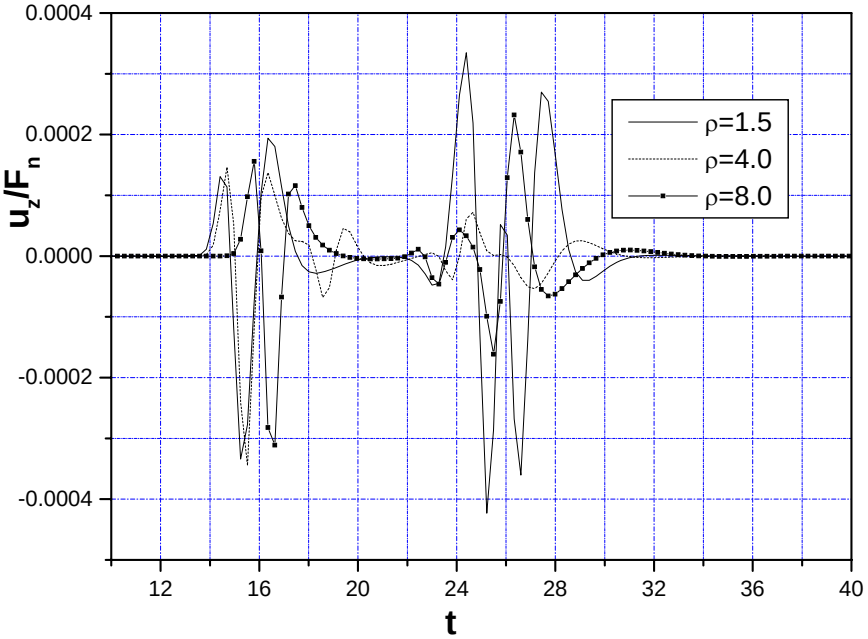

(b)

Figure 6(a)-(b): Time domain response of the points with $z = 5.0$ and $\rho = 1.5, 4.0, 8.0$ near a permeable cylindrical hole surface subjected to a normal concentrated ring load located at $z = 0.0$.

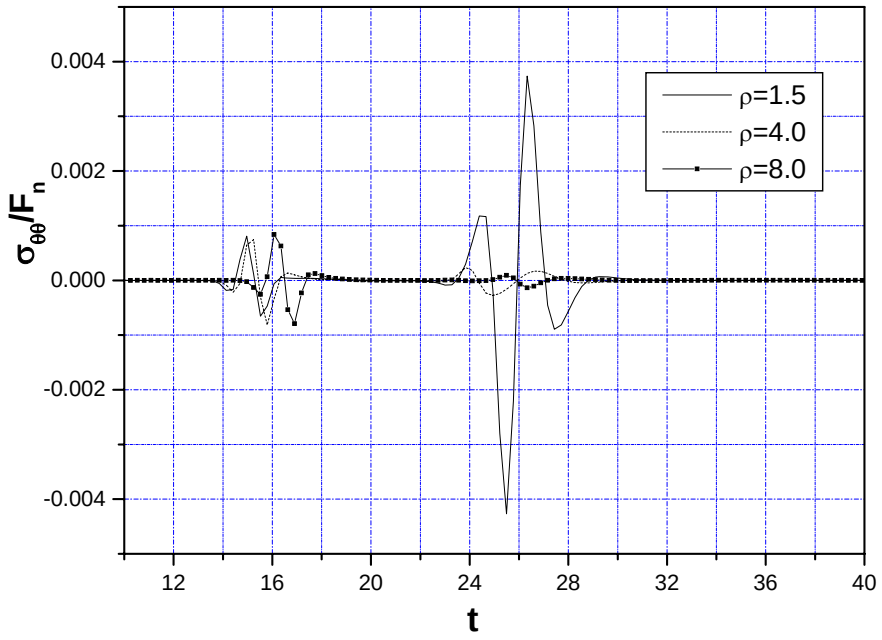

(c)

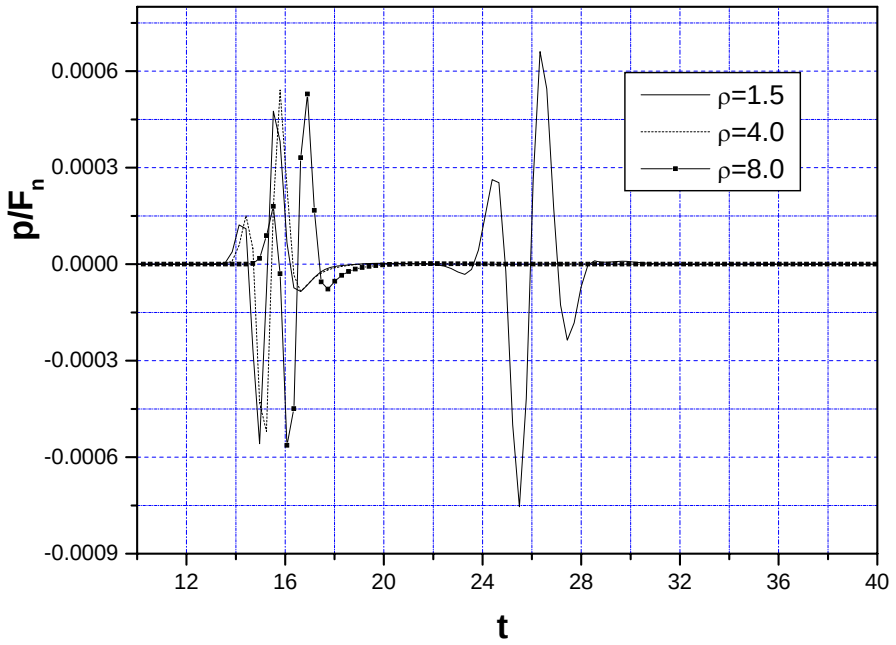

(d)

Figure 6 (c)-(d): Time domain response of the points with $z = 5.0$ and $\rho = 1.5, 4.0, 8.0$ near a permeable cylindrical hole surface subjected to a normal concentrated ring load located at $z = 0.0$.

5 Conclusions

In this paper, a closed form solution in the frequency-wave-number domain for a cylindrical hole subjected to a concentrated and a uniformly distributed ring load is derived. The frequency domain solution is obtained by inversion of the Fourier transformation with respect to the axial wave number, while the time-space domain solution is recovered by double inversion of the Fourier transformation with respect to frequency as well as the axial wave number. The numerical results conclude that the dynamic response of the porous medium around the hole depends on many factors such as the parameters of porous media, the location of receivers, the boundary conditions along the hole surface as well as the characteristics of the loads. It should be noted that for different physical variables, the resonance frequencies of the porous medium are quite different. Consequently, signals with different central frequency should be used if maximums of different physical variables are expected to be observed. The pseudo-Rayleigh wave along the surface of the hole has a significant influence on the dynamic response of the porous medium. However, the pore pressure due to the pseudo-Rayleigh waves can only be observed near the surface of the hole. For common values of permeability, the P2 wave only propagates over a very small distance, so it is invisible for all the calculated variables. Consequently, for geophysical borehole exploration, the P2 wave of the porous medium is less useful than other wave modes; it only dissipates some energy from the source.

As mentioned in Section 2, Biot's theory is used in this study, although it has some limitations for some cases. It is of interest to apply mixture theory or the theory of porous media (TPM) to treat the present or other problems in the future and compare the results with those from Biot's theory. This will clarify the limitations of different models.

Acknowledgments:

The project is supported by National Natural Science Foundation of China with grant number No. 50578071. The constructive comments from two referees are highly appreciated.

References

Biot, M.A. (1956a). Theory of propagation of elastic waves in a fluid-saturated porous solid, I, Low frenquency range. J Acoust Soc Am 28, 168-178.

Biot, M.A. (1956b). Theory of propagation of elastic waves in a fluid-saturated porous solid,

II: Higher frenquency range. J Acoust Soc Am 28, 179-191.

Biot, M.A. (1962). Mechanics of deformation and acoustic propagation in porous media. J Appl Phys 33, 1482-1498.

Biot, M.A. (1941). General theory of three-dimensional consolidation. J Appl Phys 12, 155-164.

Bowie, O.L. (1947). Elastic stresses due to a semi-infinite band of hydrostatic pressure acting over a cylindrical hole in an infinite solid. Q Appl Math 5, 100-101.

Bowen, R.M. (1980). Incompressible porous media models by use of the theory of mixtures. Int J Eng Sci 18, 1129-1148.

Bowen, R.M. (1982). Compressible porous media models by use of the theory of mixtures. Int J Eng Sci 20, 697-735.

Christensen, R.M. (1979). Mechanics of Composite Materials. Wiley Interscience, New York.

Cui, L., Cheng, A.H.D., Abousleiman, Y. (1997). Poroelastic solution for an inclined borehole. ASME J Appl Mech 64, 32-38.

de Boer, R. (2000) Theory of Porous Media—Highlights in the Historical Development and Current State. Springer, New York.

Ehlers, W., Bluhm, J. (2002). Porous media: theory, experiments, and numerical applications. New York : Springer.

Hudson, J.A., Liu, E. & Crampin, S. (1996). The mechanical properties of materials with interconnected cracks and pores. Geophys J Int 124, 105–112.

Jakobsen, M., Johansen, T.A., McCann, C. (2003). The acoustic signature of fluid flow in complex porous media. J Appl Geophys 54, 219-246.

Johnson, D.L., Koplik, J., Dashen, R. (1987). Theory of dynamic permeability and tortuosity in fluid-saturated porous-media. J Fluid Mech 176, 379-402.

Jordan, D.W. (1962). The stress wave from a finite cylindrical explosive source. J Math Mech 11, 503-551.

Morland, L.W. (1972). A simple constitutive theory for a fluid-saturated porous solid. J Geophys Res 77, 890– 900.

Mura, T. (1982). Micromechanics of Defects in Solids.Martinus-NijhoK, Dordrecht.

Nemat-Nasser, S., Hori, M.: Micromechanics (1999). Overall Properties of Heterogeneous Materials, 2nd Revised Edition.North-Holland, Amsterdam.

O'Connell, R.J., Budiansky, B. (1977). Viscoelastic properties of fluid-saturated cracked solids . J Geophys Res 82, 5719-5735.

Oppenheim, A.V., Schafer, R.W. (1999). Discrete-time signal processing. Prentice-Hall Inc, Englewood Cliffs, NJ.

Parnes, R. (1969). Response of an infinite elastic medium to traveling loads in a cylindrical bore. ASME J Appl Mech 36, 51-58.

Parnes, R. (1986). Steady-state ring-load pressure on a borehole surface. Int J Solids Structures 22, 73-86.

Parnes, R. (1983a). Elastic response to a time-harmonic torsion-force acting on a bore surface. Int J Solids Structures 19, 925-934.

Parnes, R. (1983b). Applied tractions on the surface of an infinite cylindrical bore. Int J Solids Structures 19, 165-177.

Passman, S.L., Nunziato, E.W., Walsh, E.K. (1984). A theory of multiphase mixtures, Appendix in: Truesdell, C.A. (Ed.), Rational Thermodynamics, Hopkins University Press, pp.286-325, 2nd ed.

Pride, S.R., Morgan, F.D., Gangi, A.F. (1993). Drag forces of porous-medium acoustics. Phys Rev B 47, 4964-4978.

Rajapakse, R.K.N.D. (1983). Stress analysis of borehole in poroelastic medium. ASCE J Eng Mech 119, 1205-1227.

Ricker, N.H. (1977). Transient waves in visco-elastic media. Elsevier, Amsterdam.

Selberg, W.L. (1952). Transient compression waves from spherical and cylindrical cavities. Ark Fys 5, 97-108.

Sneddon, I.N. (1951). Fourier transforms. McGraw-Hill Book Co Inc, New York.

Tranter, C.J.: (1946). On the elastic distortion of a cylindrical hole by a localized hydrostatic pressure. Q Appl Math 4, 298-302.

Truesdell, C., Noll, W. (1965). The non-linear field theories of mechanics. In: Flügge, S.(Ed.), Principles of Classical Mechanics and Field Theory, Handbuck der Physik, Vol.III/3. Springer, New York.

Appendix

The three constants $A(\omega,\xi)$, $B(\omega,\xi)$, $C(\omega,\xi)$ for a concentrated ring normal load F_n are given as follows

$$A(\omega,\xi)=\frac{\tilde{F}_n(\omega)}{2\pi R\Pi(\xi,\omega)}\gamma_t H_{0sR}^{(2)}H_{1tR}^{(2)}(k_f^2-k_s^2)k_s^2(\alpha-k_s^2\varepsilon_1+\varepsilon_2)(\xi^2-\gamma_t^2) \tag{A.1}$$

$$B(\omega,\xi)=-\frac{\tilde{F}_n(\omega)}{2\pi R\Pi(\xi,\omega)}\gamma_t H_{0fR}^{(2)}H_{1tR}^{(2)}k_f^2(\alpha-k_f^2\varepsilon_1+\varepsilon_2)(\gamma_t^2-\xi^2) \tag{A.2}$$

$$\begin{aligned}C(\omega,\xi)=\frac{i\xi\tilde{F}_n(\omega)}{\pi R\Pi(\xi,\omega)}\delta(\omega+\xi v)\Big[&\gamma_s H_{0fR}^{(2)}H_{1sR}^{(2)}k_f^2(\alpha-k_f^2\varepsilon_1+\varepsilon_2)\\&-(\alpha+\varepsilon_2)\gamma_f k_s^2 H_{0sR}^{(2)}H_{1fR}^{(2)}+\varepsilon_1\gamma_f k_s^4 H_{0sR}^{(2)}H_{1fR}^{(2)}\Big]\end{aligned} \tag{A.3}$$

$$\begin{aligned}\Pi(\xi,\omega)=\gamma_t\Big\{&-2\gamma_f k_s^2 H_{0sR}^{(2)}H_{1fR}^{(2)}(k_t^2H_{1tR}^{(2)}-2\xi^2\gamma_t RH_{0tR}^{(2)})\mu(\alpha-k_s^2\varepsilon_1+\varepsilon_2)\\&+H_{0fR}^{(2)}\Big[2\gamma_s k_f^2H_{1sR}^{(2)}(-2\xi^2\gamma_t RH_{0tR}^{(2)}+k_t^2H_{1tR}^{(2)})\mu(\alpha-k_f^2\varepsilon_1+\varepsilon_2)\\&-RH_{0sR}^{(2)}H_{1tR}^{(2)}(2\xi^2-k_t^2)\Big\langle 2\mu\gamma_f^2k_s^2(\alpha-k_f^2\varepsilon_1+\varepsilon_2)\\&+k_f^4\varepsilon_1(+\mu\gamma_s^2+\lambda k_s^2)+k_f^2\left(2\mu\gamma_s^2(\alpha+\varepsilon_2)+\lambda\varepsilon_1k_s^4\right)\Big\rangle\Big]\Big\}\end{aligned} \tag{A.4}$$

where $H_{nfR}^{(2)}\equiv H_n^{(2)}(\gamma_f R)$, $H_{nsR}^{(2)}\equiv H_n^{(2)}(\gamma_s R)$ and $H_{ntR}^{(2)}\equiv H_n^{(2)}(\gamma_t R)$, $n=0,1$.

[#] Part of this report forms the manuscript: Lu, J.-F. and Jeng, D.-S. (2006): Dynamic analysis of an infinite cylindrical hole in a saturated poroelastic medium. *Archive of Applied Mechanics* (accepted).